STRENGTH
AND PLASTICITY

Study of the Effect of Carbon on the Deformation Behavior and Microstructure of a Ti−10V−2Fe−3Al Alloy

A. V. Zhelnina[a], *, M. S. Kalienko[a, b], and N. V. Shchetnikov[a]

[a]*PSC VSMPO-AVISMA Corporation, Verkhnyaya Salda, 624760 Russia*
[b]*Ural Federal University n.a. the First President of Russia B.N. Yeltsin, Ekaterinburg, 620002 Russia*
*e-mail: avzhelnina@gmail.com

Abstract—Scanning electron microscopy (SEM) and X-ray diffraction (XRD) analysis are used to study the structure, phase composition, and deformation behavior of a titanium Ti−10V−2Fe−3Al alloy with different carbon contents. It is shown that as the carbon content in the alloy increases to the maximum carbon solubility, the dispersity of the secondary α-phase increases and, therefore, the strength of the alloy increases. After reaching the carbon solubility limit, titanium carbide particles are observed in the alloy structure; the morphology of the particles and their sizes are similar to those of the primary α-phase. The titanium carbide particles do not affect the strength and plasticity characteristics of the alloy during tensile tests and retain their initial shape after deformation. At the stage of strain localization, titanium carbide particles are sites of micropore nucleation.

Keywords: Ti−10V−2Fe−3Al titanium alloy, ultimate strength, microstructure, titanium carbide

DOI: 10.1134/S0031918X21020101

INTRODUCTION

Owing to the combination of mechanical properties (specific strength, fracture toughness, and fatigue strength), transition-class titanium $(\alpha + \beta)$-alloys, the Ti−10V−2Fe−3Al alloy among them, are widely used in aircraft industry for manufacturing high-strength structural elements of airframe and landing gear [1, 2]. Specification requirements for the chemical composition of the alloy strictly limit the contents of light elements in the alloy, namely, the content of oxygen, nitrogen, carbon, and hydrogen is no more than 0.13, 0.05, 0.05, and 0.015 wt %, respectively [3]. The radius of the oxygen, nitrogen, carbon, and hydrogen atoms are 60, 71, 77, and 46 pm, respectively. Because of this, they occupy interstices in the titanium crystal lattice (the radius of octahedral pores in α-Ti is 61 pm; the radius of tetrahedral pores in α-Ti and β-Ti is 33 and 44 pm, respectively). Similarly to oxygen and nitrogen, carbon in titanium alloys is the α-stabilizer and extends the temperature range of α-phase stability [4, 5]. The carbon solubility in titanium is substantially lower than the nitrogen and oxygen solubilities; the maximum solubility of carbon in the α-phase is ~0.48 wt % (2 at %). The carbon solubility in titanium alloys depends on the chemical and phase compositions of the alloy [6]. For example, the solubility limit of carbon in the widely used Ti6Al4V alloy is ~0.35 wt %; the solubility limit in β-titanium alloys is substantially lower and is 0.006 and 0.023 wt % in the Ti15Mo and

Ti16Nb alloys, respectively [7]. When the carbon content in the crystal lattice exceeds the solubility limit, carbon and titanium form a new phase that is titanium carbide [8]. The Ti_xC_y phase can have different stoichiometry and, therefore, different physico-mechanical properties. The TiC titanium carbide has a high melting temperature (3140°C) and a substantially higher modulus of elasticity (440 GPa) compared to that of structural titanium alloys (115 GPa).

Some of the first data on the effect of carbon on the properties of titanium were reported in 1955 [4]. It was found that the effect of carbon on the properties is substantially lower than that of oxygen and nitrogen, although the radius of carbon atom is higher [4]. The lower strengthening effect of carbon compared to that of nitrogen and oxygen is explained by lower bonding forces of carbon atoms with dislocations compared to those in the Ti−O and Ti−N systems. Strength characteristics of titanium enhance as the carbon content increases to 0.3 wt %; after that, they are almost independent of the carbon content. In the range of low carbon concentrations (to 0.3 wt %), the 0.01 wt % carbon addition increases the ultimate tensile strength and yield strength of α-titanium by ~7 MPa [9]. The similar effect of carbon is also observed for alloyed titanium compositions [10]. However, the high carbon content, of more than 0.5 wt %, substantially decreases the plasticity, fracture toughness, and fatigue resistance. Nevertheless, studies investigating the effect of

Table 1. Chemical composition of the Ti−10V−2Fe−3Al alloys under study

Carbon content, wt %	Oxygen content, wt %	Al$_{str.eq}$	Mo$_{str.eq}$
0.008	0.11	4.3	11.10
0.034	0.10	4.49	11.30
0.063	0.10	4.73	11.27

carbon on the mechanical properties and deformation behavior of titanium alloys are continuing [11−17]. In particular, new data on the process-related plasticity of the Ti6Al4V alloy with 0.77 wt % C in a temperature range of 900−1100°C were obtained in [11]. It was found in [12] that carbon and boron additions in metastable β-alloys (Ti-15333, Ti-1023, Ti-5553) decrease the size of β- and fine α-phase grains; the effect of these additions on the strength and plasticity was determined. The favorable effect of carbon (0.23 wt %) on the strength and creep resistance of the Ti−8Al−1Mo−1V alloy was demonstrated in [13]. Data on the effect of carbon on the deformation behavior of alloys were reported in [16−20]; changes in the microstructure of samples in the plastic strain range were studied after tensile testes. However, there are few studies related to the effect of carbon, whose content is close to its maximum solubility, on the deformation behavior of transition-class (α + β)-titanium alloys. In our previous study [16], it was found that, as the carbon content increases to the carbon solubility limit, the strength of the Ti−10V−2Fe−3Al alloy increases.

The aim of the present study is to investigate the deformation behavior of the Ti−10V−2Fe−3Al alloy, whose carbon contents are lower and higher than the carbon solubility limit in the alloy, and to determine the nature of variations of mechanical properties.

EXPERIMENTAL

As the material for the investigation, we used Ti−10V−2Fe−3Al (wt %) alloy rods 22 mm in diameter, which were manufactured at the PSC VSMPO-AVISMA Corporation. We studied three compositions differing in carbon content; the carbon content determined by atomic emission spectroscopy was 0.008, 0.034, and 0.063 wt % (Table 1). The mechanical

properties of samples were studied for the heat-treated state. The first stage of heat treatment included water quenching from the (α + β)-region from a temperature below the polymorphous transformation temperature by 45°C; the second stage is aging at 500°C for 8 h.

Tensile tests were performed at room temperature in accordance with the ASTM E8 Standard [20] using a Zwick Z600 tension testing machine. Two samples were studied for each state.

The microstructure of longitudinal sections of rods was studied using microsections, the mirror surface of which was prepared by polishing with colloid silicon oxide. A Quanta 3D FEG scanning electron microscope equipped with a back-scattered electron detector (BSED, Z contrast), an electron backscatter diffraction (EBSD) detector, and an EDAX Genesis 2000 electron microprobe analyzer was used.

X-ray diffraction (XRD) analysis of samples was performed at a step of 0.01° and 0.5-s exposition per point using a Bruker D8 Advance diffractometer equipped with a LynxEye detector; the operating voltage was 40 kV and the current was 40 mA.

The JMatPro software was used to simulate structural and phase transformations in the alloy under study.

RESULTS AND DISCUSSION

The microstructure of the quenched and aged Ti−10V−2Fe−3Al alloy is characterized by the presence of the primary α-phase (α$_I$) with globular morphology and an average particle size of 2−3 μm and the fine secondary α-phase (α$_{II}$) with lamellar morphology (Fig. 1). Subgrains of the β-phase 2 to 5 μm in size are observed, which were formed at the stage of deforma-
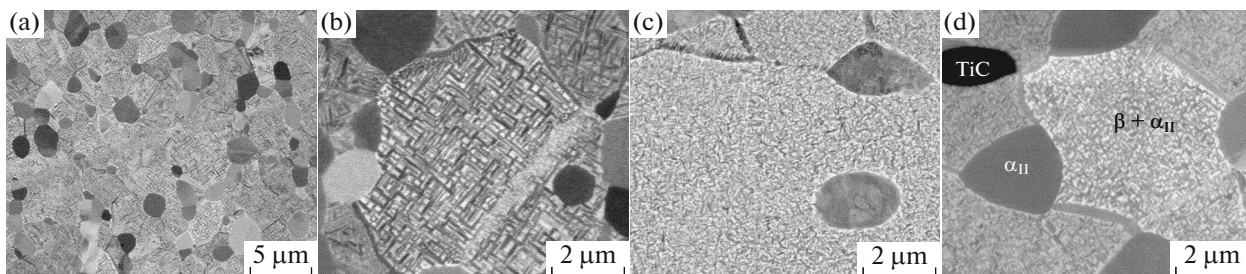

Fig. 1. Electron micrographs (SEM) of the Ti−10V−2Fe−3Al samples with (a, b) 0.008, (c) 0.034, and (d) 0.063 wt % C.
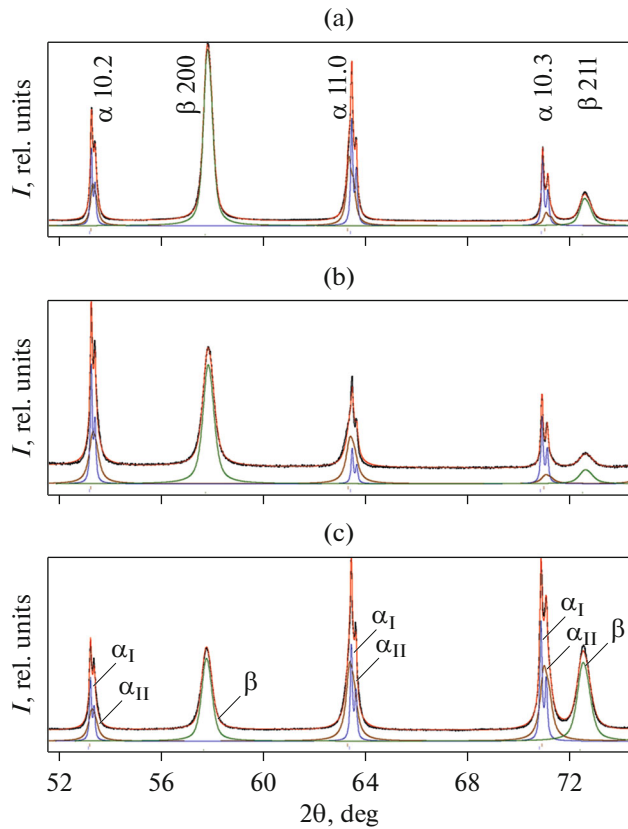
Fig. 2. X-ray diffraction patterns and profiles of reflections of some phases in samples with (a) 0.008, (b) 0.034, and (c) 0.063 wt % C.

tion of rods in the ($\alpha + \beta$)-region and are decorated by the secondary α-phase during aging.

The study of the microstructure of the aged samples with different carbon contents allowed us to find difference in the dispersity of the secondary α-phase present in the alloy structure; this is related to the effect of carbon on the intensity of the decomposition of the metastable β-phase. The increase in the dispersity of products of the decomposition of the supersaturated β-solid solution was observed in adding carbon in a number of works [12, 23]. The secondary-phase plate thickness was estimated by Full Profile analysis of XRD patterns [24].

Figure 2 shows X-ray diffraction patterns with fitting profiles for some phases. According to the data

obtained, the secondary α-phase plate thickness in the samples with 0.008, 0.034, and 0.063 wt % carbon is 47, 27, and 33 nm, respectively. In turn, the increase in dispersity of the secondary α-phase affects the alloy properties, namely, leads to the enhance in the strength characteristics at the expense of increasing amount of interphase boundaries and decreasing the dislocation movement path [25, 26]. Table 2 gives the results of the XRD analysis of the samples. The increase in the content of interstitial element, carbon, leads to the extend of crystall lattice; in particular, the lattice parameter c of the α-phase increases. The data obtained agree with the literature data [9].

After heat treatment of samples with a carbon content of 0.063 wt %, globular particles of a third phase (with a volume fraction of less than 5%) were found within β-grains and at β-grain boundaries. The morphology of the particles is identical to that of the primary α-phase. However, when studying the particles in the backscattered electron mode, they are characterized by dark contrast; the study of the particles in the secondary electron mode demonstrates their volume contour (Figs. 3a, 3c). As is known, when a structure is studied using the backscattered electron mode, the higher the difference between the densities of structural elements (between the numbers of chemical elements), the more substantial the difference in the contrast of structural elements. This is related to the higher amount of electrons reflected from an area having the higher density (the higher atomic number of chemical elements). This leads to the formation of the brighter image of this area. The density of β-phase is higher than that of the α-phase, since the β-phase is characterized by the higher content of β-stabilizers (elements with the high atomic number) and the lower aluminum content compared to that in the α-phase. Therefore, in images taken with the backscattered electrons, the β-phase has a brighter contrast compared to that of the α-phase. Since the carbon content in the titanium carbide is higher and its density is lower as compared to that of the α-phase, titanium carbide particles are characterized by darker contrast compared to that of the α-phase.

The chemical composition of third phase particles (Fig. 3a) was studied by electron microprobe analysis. The intensity of spectrum lines in the energy range corresponding to carbon is higher than that for the neighboring area of metal (Fig. 3b). However, no

Table 2. Lattice parameters of the Ti−10V−2Fe−3Al alloys under study

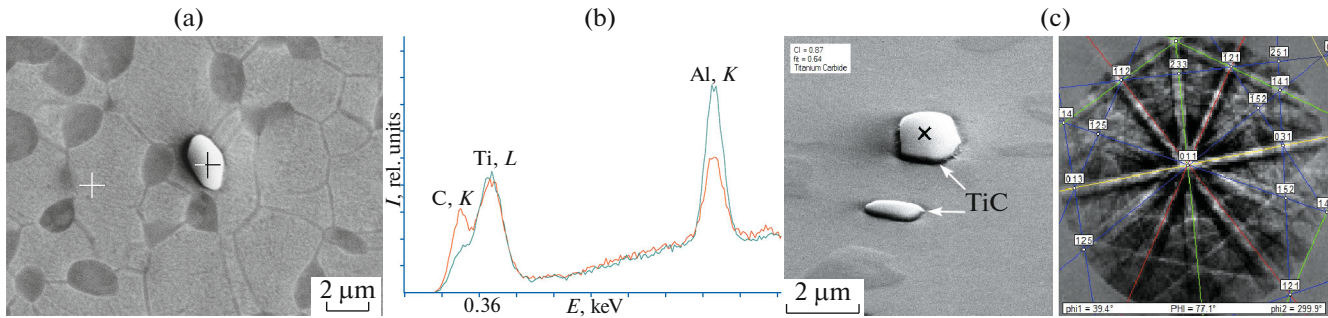| Carbon content, wt %	β-phase	Primary α-phase			Secondary α-phase			
	a_β, Å	a, Å	c, Å	c/a	a, Å	c, Å	c/a	d, nm
0.008	3.190	2.930	4.675	1.595	2.935	4.662	1.588	46.7
0.034	3.190	2.930	4.677	1.596	2.934	4.664	1.590	27.4
0.063	3.193	2.932	4.680	1.596	2.934	4.670	1.591	33.3

Fig. 3. (a) Areas of chemical analysis, (b) X-ray diffraction patterns, and (c) Kikuchi line pattern taken with EBSD analysis of titanium carbide particles in the Ti−10V−2Fe−3Al alloy with 0.063 wt % C.
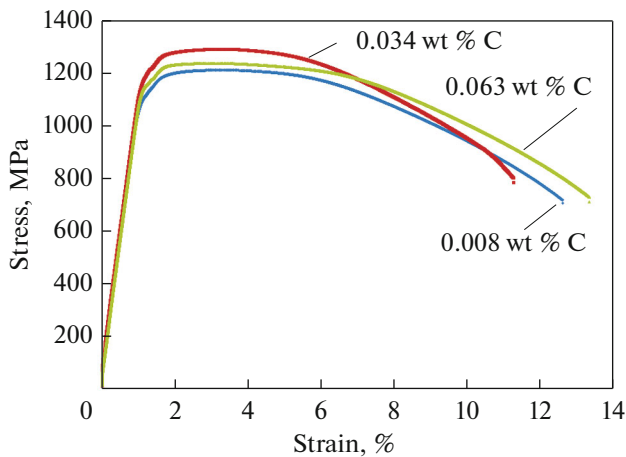

Fig. 4. Stress-strain curves measured during tensile tests of the Ti−10V−2Fe−3Al alloy.

additional reflections in X-ray diffraction pattern, besides the reflections of the α- and β-phases, were found (Fig. 2c). The absence of reflections typical of the titanium carbide in the X-ray diffraction pattern is explained by the low volume fraction (less than 5%) of third-phase particles in the structure. The study of the microstructure of samples using EBSD analysis allowed us to take the diffraction pattern for the third-phase particles (Fig. 3c), which is characterized by Kikuchi lines; the found third-phase particles are identified to be the TiC titanium carbide; however, its chemical composition should be refined.

The computer simulation of structural and phase transformations using the JMatPro software allowed us to calculate the limit of carbon solubility in the Ti−10V−2Fe−3Al alloy, which is 0.053 wt %. Thus, the presence of observed titanium carbide particles in the structure of alloy with 0.063 wt % carbon is confirmed by the computer simulation data.

Figure 4 shows stress−strain curves which were measured during tensile tests of the Ti−10V−2Fe−3Al samples. Three characteristic areas can be selected in all these curves: these are the elastic strain area, of the

abrupt stress enhance with increasing strain, and uniform elongation area, in which the stress changes insignificantly, and the area corresponding to the formation of neck in the sample, when the stress begins to decrease abruptly.

Table 3 shows the strength and plasticity characteristics of the Ti−10V−2Fe−3Al alloys with carbon contents of 0.008 to 0.063 wt %. The obtained range of mechanical characteristics is typical of the Ti−10V−2Fe−3Al alloy subjected to the aforementioned heat treatment. However, it should be noted that the final combination of mechanical properties of the alloy, among other things, is affected by the deformation route of half-product [27]. As the carbon content increases from 0.008 to 0.034 wt % (by 0.026 wt %), the yield strength increases by 73 MPa (see Table 3). However, at a carbon content of 0.063 wt %, the yield strength decreases by 30 MPa, whereas the relative elongation is higher by 2% compared to that for a carbon content of 0.034 wt %. This is likely to be related to the precipitation of titanium carbide particles, the formation of which leads to the decrease in the dispersity of the secondary α-phase. The analysis of the data given in Table 2 allows us to state that the carbon content in the primary and secondary α-phases of the alloy with 0.063 wt % carbon is higher than that in the alloy containing 0.034 wt % carbon.

Using the Hall−Petch equation [28], we calculated the yield strength of the alloy as a function of d:

$$\sigma = \sigma_0 + kd^{-1/2}, \qquad (1)$$

Table 3. Mechanical properties of the Ti−10V−2Fe−3Al alloys

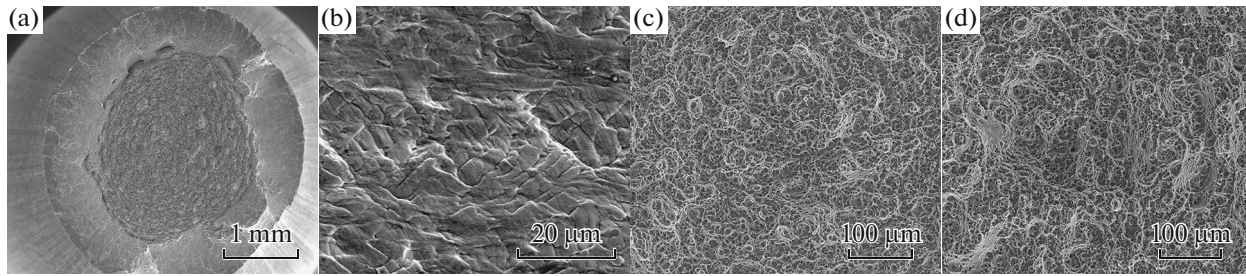| Carbon content, wt %	$\sigma_{0.2}$, MPa	σ_u, MPa	δ, %
0.008	1121	1213	12.6
0.034	1194	1280	11.3
0.063	1164	1238	13.5

Fig. 5. (a, b) Fracture and forming surface of the sample with 0.063 wt % C after tensile tests and the morphology of fractures of samples with (c) 0.008 and (d) 0.063 wt % C.
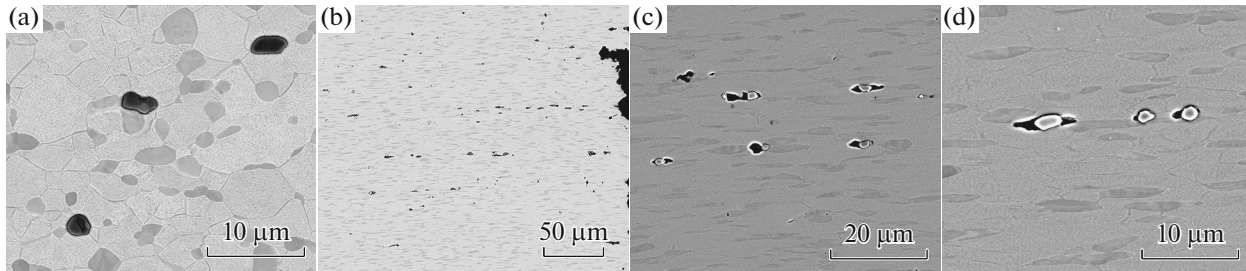

Fig. 6. Microstructure of longitudinal section of sample with 0.063 wt % C after tensile tests: (a) uniform elongation area and (b, c, d) neck area.

where σ_0 is the strain stress without the strengthening by secondary α-phase (in calculating, it is taken to be unchanged); k is the constant; and d is the secondary α-phase plate thickness determined by XRD analysis.

The calculated difference between the values of yield strength of the alloys with 0.008 and 0.034 wt % C and 0.034 and 0.063 wt % C was found to be 77 and 31 MPa, respectively. Thus, the change in the strength of the alloy, which is observed as the carbon content increases from 0.008 to 0.063 wt %, first of all is related to, changing the dispersity of the secondary α-phase.

The fractography of transverse fractures of samples indicates that no effect of the carbon content on changing the fracture surface of the Ti−10V−2Fe−3Al alloy is found (Fig. 5). No substantial differences between the samples were found; fractures of all samples are classical and typical of ductile cup-and-cone fracture with characteristic equiaxed fracture pits (Figs. 5a, 5c, 5d). No carbide particles were found in the fracture of the sample with 0.063 wt % carbon. Figure 5b shows the forming surface of this sample in the neck area, in which numerous steps, parallel slip lines (on the surface), and outlines of elongated strained structural elements are observed. This indicates the high plasticity of the metal, the main deformation mechanism of which is the intragrain dislocation glide.

Figure 6 shows the microstructure of the longitudinal section of the sample with 0.063 wt % carbon content, which was subjected to tensile tests, in the uni-

form strain region (Fig. 6a) and near the fracture (Figs. 6b−6d). In the strain localization region, the formation of micropores near carbide particles is observed (Figs. 6b−6d). Hard titanium carbide particles are characterized by substantially higher stiffness compared to that of the matrix and are the barriers for the dislocation motion, accumulate dislocations and, as a result, micropores form at the interface with the matrix upon deformation. When studying carbide particles in the uniform elongation region of samples (Fig. 6a), no micropore formation was found. This indicates a sufficiently high adhesion force between the particles and matrix. The formation of micropores and their subsequent growth during deformation depend on a great number of the parameters of material and deformation. Grain and subgrain boundaries, inclusions, interfaces, i.e., regions characterized by the high number density of dislocations are the most common places for micropore nucleation [29, 30]. After significant growth of pores, when a certain volume fraction of pores is reached, they begin to merge, and a crack forms, which results in the sample failure. The effect of inclusions and pores on peculiarities of the deformation behavior of the 10V−2Fe−3Al alloy was studied in [31]. It was found that, to a certain spacing between particles, micron-sized inclusions do not participate in the fracture process, i.e., at a certain distribution of inclusions and pores in the material, they can form nuclei which become sites for the nucleation of main crack and affect the failure upon deformation. In the case of the considered sample of the 10V−2Fe−

3Al alloy with 0.063 wt % carbon, which is characterized by carbide particles in the structure, the combination of their size and volume fraction do not affect substantially the deformation behavior of the Ti–10V–2Fe–3Al alloy. Thus, the obtained data demonstrate the mechanism of the effect of carbon on the microstructure and deformation behavior of the Ti–10V–2Fe–3Al alloy.

CONCLUSIONS

The effect of carbon on the mechanical properties and structure of high-strength titanium Ti–10V–2Fe–3Al alloy was studied in this work. As the carbon content in the alloy increases to the maximum carbon solubility, which, according to the simulation data, is 0.053 wt %, the increase in the alloy strength takes place at the expense of increasing dispersity of the secondary α-phase. After heat treatment under the studied conditions, the structure of alloy with a carbon content of 0.063 wt % is characterized by titanium carbide particles, whose morphology is similar to that of the primary α-phase. In this case, the dispersity of the secondary α-phase decreases; this leads to the decline in the strength of the alloy compared to that of the alloy containing 0.034 wt % carbon. The found correlation between the strength and dispersity of the secondary α-phase is described adequately by the Hall–Petch equation. During deformation of the alloy with 0.063 wt % carbon, titanium carbide particles are sites for the micropore nucleation at the stage of strain localization. The volume fraction of titanium carbide particles in the alloy structure is relatively low; because of this, the carbide particles do not affect the plasticity and strength characteristics of the Ti–10V–2Fe–3Al alloy during tensile tests.

REFERENCES

1. R. R. Boyer and R. D. Briggs, "The use of β titanium alloys in the aerospace industry," J. Mater. Eng. Perform. **14**, No. 6, 681–685 (2005).

2. J. D. Cotton, R. D. Briggs, R. R. Boyer, S. Tamirisakandala, P. Russo, N. Shchetnikov, and J. C. Fanning, "State of the art in beta titanium alloys for airframe applications," JOM **67**, No. 6. 1281–1303 (2015).

3. *Titanium alloy forgings 10V–2Fe–3Al, Aerospace Material Specification, ASM4984* (1987).

4. H. R. Ogden and R. I. Jaffee, Titanium Metallurgical Laboratory Report No. 20 (Ohio, 1955).

5. H. Conrad, "Effect of interstitial solutes on the strength and ductility of titanium," Prog. Mater. Sci. **26**, 123–403 (1981).

6. G. Cam, H. M. Flower, and D. R. F. West, "Constitution of Ti–Al–C alloys in temperature range 1250–750°C," Mater. Sci. Technol. **7**, No. 6, 505–511 (1991).

7. M. Yan, M. Qian, C. Kong, and M. S. Dargusch, "Impacts of trace carbon on the microstructure of as-sintered biomedical Ti–15Mo alloy and reassessment of

8. E. K. Storms, *Refractory Materials, V. 2. The Refractory Carbides* (Academic Press, New York, 1967) p. 299.

9. B. A. Kolachev, V. A. Livanov, and A. A. Bukhanova, *Mechanical Properties of Titanium and its Alloys* (Metallurgiya, Moscow, 1974) [in Russian].

10. O. P. Solonina and N. M. Ulyakova, "Effect of carbon on the mechanical properties and structure of titanium alloys," Met. Sci. Heat Treat. **16**, No. 4, 310–312 (1974).

11. A. Szkliniarz, "Deformation of Ti–6Al–4V alloy with carbon," Solid State Phenom. **176**, 149–156 (2011).

12. R. Banoth, R. Sarkar, A. Bhattacharjee, T. K. Nandy, and G. V. S. Nageswara Rao, "Effect of boron and carbon addition on microstructure and mechanical properties of metastable beta titanium alloys," Mater. Des. **67**, 50–63 (2015).

13. A. Szkliniarz, "Effect of heat treatment on the microstructure and properties of Ti–8Al–1Mo–1V alloy with carbon addition," Solid State Phenom. **229**, 131–136 (2015).

14. A. Szkliniarz, "Microstructure and properties of beta 21S alloy with 0.2 wt % of carbon," Solid State Phenom. **246**, 19–24 (2016).

15. A. V. Zhelnina, A. G. Illarionov, and A. V. Trubochkin, "Study of interstitial impurities influence on properties of titanium alloy Ti–5Al–5V–5Mo–3Cr–1Zr," Solid State Phenom. **284**, 460–464 (2018).

16. A. V. Zhelnina, A. G. Illarionov, M. S. Kalienko, A. A. Popov, and N. V. Schetnikov, "Effect of carbon content on the structure and mechanical properties of TI–10V–2Fe–3Al alloy," *XIX International scientific-technical conference "The Ural school-seminar of metal scientists-young researchers" KnE Engineering* (2019) pp. 170–175.

17. S. Zhang, W. Zeng, X. Gao, D. Zhou, and Y. Lai, "Role of titanium carbides on microstructural evolution of Ti–35V–15Cr–0.3 Si–0.1 C alloy during hot working," J. Alloys Compd. **684**, 201–210 (2016).

18. Z. Q. Chen, D. Hu, M. H. Loretto, and X. Wu, "Influence of 0.2 wt % C on the aging response of Ti–15–3," Mater. Sci. Technol. **20**, No. 6, 756–764 (2004).

19. L. -H. Chen, P. A. Blenkinsop, and I. P. Jones, "Effects of boron, carbon, and silicon additions on microstructure and properties of a Ti–15Mo based beta titanium alloy," Mater. Sci. Technol. **17**, No. 5, 573–580 (2001).

20. R. Sarkar, P. Ghosal, K. Muraleedharan, T. K. Nandy, and K. K. Ray, "Effect of boron and carbon addition on microstructure and mechanical properties of Ti–15–3 alloy," Mater. Sci. Eng., A **528**, No. 13–14, 4819–4829 (2011).

21. *ASTM E8/8M–16a. Standard test methods for tension testing of metallic materials. American Society for Testing and Materials* (Annual book of ASTM Standards, 2016).

22. *TOPAS. V3, General Profile and Structure Analysis Software for Powder Diffraction Data. User's manual. Karlsruhe* (Bruker AXS, Germany, 2005).

23. N. Wain, X. Hao, G. A. Ravi, and X. Wu, "The influence of carbon on precipitation of α in Ti–5Al–5Mo–

5V−3Cr," Mater. Sci. Eng., A **527**, Nos. 29−30, 7673−7683 (2010).

24. M. S. Kalienko, A. V. Volkov, and A. V. Zhelninav, "Use of full-profile X-ray analysis for estimation of the dispersity of the secondary alpha phase in high-strength titanium alloys," Crystallogr. Rep. **65**, No. 3, 412−416 (2020).

25. T. Hamajima, G. Lutjering, and S. Weissmann, "Importance of slip mode for dispersion-hardened β-titanium alloys," Metall. Trans. **4**, No. 3, 847−856 (1973).

26. M. S. Kalienko, A. V. Volkov, V. A. Kropotov, M. A. Konovalov, and V. A. Dukhtanov, "Primary α-phase VST5553 alloy with lamellar structure properties effect," *Titanium'2011: Science and technology. Proc. 12-th Int. Conf. of Titanium* (Beijing, 2011) pp. 1303−1311.

27. G. Srinivasu, Y. Natraj, A. Bhattacharjee, T. K. Nandy, and G. V. S. Nageswara Rao, "Tensile and fracture toughness of high strength b Titanium alloy, Ti−10V−2Fe−3Al, as a function of rolling and solution treat-ment temperatures," J. Mater. Des. **47**, 323−330 (2013).

28. N. J. Petch, "The cleavage strength of polycrystals," J. Iron Steel Inst. **174**, 25−28 (1953).

29. G. T. Terlinde, T. W. Duerig, and J. C. Williams, "Microstructure, tensile deformation, and fracture in aged Ti 10V−2Fe−3Al," Metall. Trans. A **14**, No. 10, 2101−2115 (1983).

30. J. W. Hutchinson and V. Tvergaard, "Softening due to void nucleation in metals," In *Fracture Mechanics: Perspectives and Directions (Twentieth Symposium)* (ASTM Int., 1989), pp. 61−83.

31. N. R. Moody, W. M. Garrison, J. E. Costa, and J. E. Smugeresky, "The role of defect size on the fracture toughness of powder processed Ti−10V−2Fe−3Al," Scr. Metall. **23**, No. 7, 1147−1150 (1989).

Translated by N. Kolchugina